Available online at www.sciencedirect.com

ScienceDirect

Ceramics International 41 (2015) 14299–14305

CERAMICS INTERNATIONAL

www.elsevier.com/locate/ceramint

Phase composition, densification and electrical conductivity of $La_{0.9}Sr_{0.1}Ga_{0.8}Mg_{0.2}O_{3-\delta}$ consolidated by the two-stage sintering method

S.L. Reis*, E.N.S. Muccillo

Energy and Nuclear Research Institute – IPEN, PO Box 11049, Sao Paulo 05422-970, Brazil

Received 4 June 2015; accepted 10 July 2015
Available online 17 July 2015

Abstract

The influence of the method of sintering on densification, phase assemblage and electrical conductivity of Sr- and Mg-doped lanthanum gallate was investigated aiming to optimize the sintering process of this solid electrolyte. Powder mixtures were prepared by solid state reactions, and the sintering of green compacts was carried out by the two-stage method varying the temperature of the first stage (T_1) and the isothermal temperature (T_2) and time (t_2) profile. The type and content of predominant impurity phases depend on specific parameters of the sintering process. In the first stage of sintering, the content of impurity phases, such as $LaSrGaO_4$ and $La_4Ga_2O_9$, decreases with increasing temperature. The relative density of sintered specimens reaches 99% whenever T_1 is 1500 °C. The mean grain size varies from 1.45 to 4.9 μm. At 600 °C the electrical conductivity attains 12 mS cm^{-1} for T_1 1400 °C and T_2 1350 °C for 5 h, with activation energy of approximately 1 eV.

Keywords: A. Sintering; C. Electrical conductivity; D. Perovskites; E. Fuel cells

1. Introduction

Lanthanum gallate with partial substitutions by strontium and magnesium has been extensively investigated over the last two decades because of its high ionic conductivity (170 mS cm^{-1} at 800 °C), negligible electronic conductivity, and good chemical stability in a wide range of oxygen partial pressures (1–10^{-22} atm) [1,2]. Doped lanthanum gallate is a promising ceramic material for application as solid electrolyte in solid oxide fuel cells operating at intermediate temperatures (600–800 °C) [2,3]. The main disadvantage of this solid electrolyte is related to secondary or impurity phases, usually detected in sintered materials regardless the method of preparation.

$La_{1-x}Sr_xGa_yMg_{1-y}O_{3-\delta}$ compositions prepared by solid state reactions may exhibit impurity phases, mainly $La_4Ga_2O_9$, $LaSrGaO_4$, $LaSrGa_3O_7$ and MgO [4–7]. The total amount of these phases is known to vary according to several factors, including the Sr content. Among the most investigated compositions, $La_{0.9}Sr_{0.1}Ga_{0.8}Mg_{0.2}O_{3-\delta}$, hereafter named LSGM, is known to contain comparatively small fractions of impurity phases.

Recently, special attention has been given to the sintering of LSGM by non conventional methods. Liu et al. [8] synthesized the $La_{0.9}Sr_{0.1}Ga_{0.8}Mg_{0.2}O_{3-\delta}$ compound by the combustion method and the consolidation of bulk specimens was carried out by spark plasma sintering. The main results show that high relative densities (~95%) along with low contents of impurity phases were obtained after sintering at 1300 °C, with electrical conductivity of approximately 7.5 mS cm^{-1} at 600 °C. Zhang et al. [9] prepared the same compound by the rapid solidification method and obtained LSGM specimens with 98% of relative density and high electrical conductivity (about 27 mS cm^{-1} at 600 °C). In a previous work we have synthesized nanopowders of LSGM by the cation complexation technique; bulk specimens were obtained by fast firing at 1400–1500 °C for 5 and 10 min. The relative density of the sintered specimens was only 90%, but the content of impurity phases was negligible [10].

In 2000, Chen and Wang [11] proposed a new method of sintering, named two-stage sintering (tss), that allowed for

*Correspondence to: Center of Materials Science and Technology, Energy and Nuclear Research Institute – IPEN, PO Box 11049, S. Paulo, 05422-970, SP, Brazil. Tel.: +55 11 31339203.
E-mail address: shirley.reis@usp.br (S.L. Reis).

http://dx.doi.org/10.1016/j.ceramint.2015.07.061
0272-8842/

obtaining yttria with high density and fine grain size. In that method, the green compact is heated up to a high temperature (T_1) at which it remains for a short (or null) holding time (t_1). Subsequently, the compact is fast cooled down to a specific temperature (T_2) for a long holding time (t_2). To improve the overall process, sufficiently high T_1 is chosen such that the compact reaches 75–85% of relative density in the first stage of sintering [12]. This method has been applied with success for sintering a number of functional ceramics such as Al_2O_3, ZnO, $BaTiO_3$, Si_3N_4, SiC, $Ca_3MgSi_2O_8$ and yttria-stabilized zirconia [13–22]. In all these studies, the main purpose was to obtain high densification along with negligible grain growth in the second stage.

In this work, LSGM powder was prepared by solid state reactions and the sintering of compacts was accomplished by the two-stage sintering method, aiming to evaluate the final densification and the electrical conductivity of the solid electrolyte. Other objective was to investigate the effect of the sintering method on phase evolution of $La_{0.9}Sr_{0.1}Ga_{0.8}Mg_{0.2}O_{3-\delta}$.

2. Experimental

2.1. Sample preparation

The compound $La_{0.9}Sr_{0.1}Ga_{0.8}Mg_{0.2}O_{2-\delta}$ was prepared by solid state reactions starting with La_2O_3 (99.9%, Alfa Aesar), $SrCO_3$ (P.A., Vetec), Ga_2O_3 (99.99%, Alfa Aesar) and MgO (P.A., Merck). The La_2O_3 precursor powder was at first heat treated at 1000 °C for 3 h. Stoichiometric amounts of the starting reagents were mixed together and calcined at 1250 °C for 4 h. This calcination step was repeated twice with intermediate grindings. After calcination, the mixture was attrition milled for 1 h with zirconia balls (ϕ 2 mm) in alcoholic medium. The dried mixture was uniaxial followed by cold isostatic (200 MPa) pressing into pellets (ϕ 10 mm and 2–3 mm thickness). The sintering process was carried out in a box-type furnace (Lindberg BlueM) with heating and cooling rates of 10 and 30 °C min^{-1}, respectively.

In the first series of experiments, the sintering temperature T_1 was varied from 1250 to 1500 °C. Subsequently T_1 was fixed at 1400 or 1500 °C and T_2 varied from 1250–1450 °C with t_2 fixed a 5 h. In all experiments the holding time t_1 was null. This procedure is hereafter called TSS

2.2. Sample characterization

The apparent density of sintered specimens was determined by the immersion method with distilled water and compared to the theoretical density (6.67 g cm^{-3}, ICSD 51-288). Structure evaluation was performed by X-ray diffraction, XRD (Bruker-AXS, D8 Advance) with Cu K_α radiation (λ=1.5405 Å) in the 20–80° 2θ range, with 0.05° step size and 2 s counting time. Identification of impurity phases was performed according to the corresponding powder diffraction files: ICDD 24-1208 ($LaSrGaO_4$), ICDD 45-0637 ($LaSrGa_3O_7$) and ICDD 37-1433 ($La_4Ga_2O_9$). The amount of impurity phases was not quantitatively determined, but the XRD patterns were normalized for the most intense reflection of the orthorhombic phase, for comparison purpose.

Microstructure observations were performed by field emission scanning electron microscopy (FESEM, FEI, Inspect F-50). The mean grain size was estimated by the intercept method [23]. Electrical resistance measurements were carried out by impedance spectroscopy (HP 4192A) in the

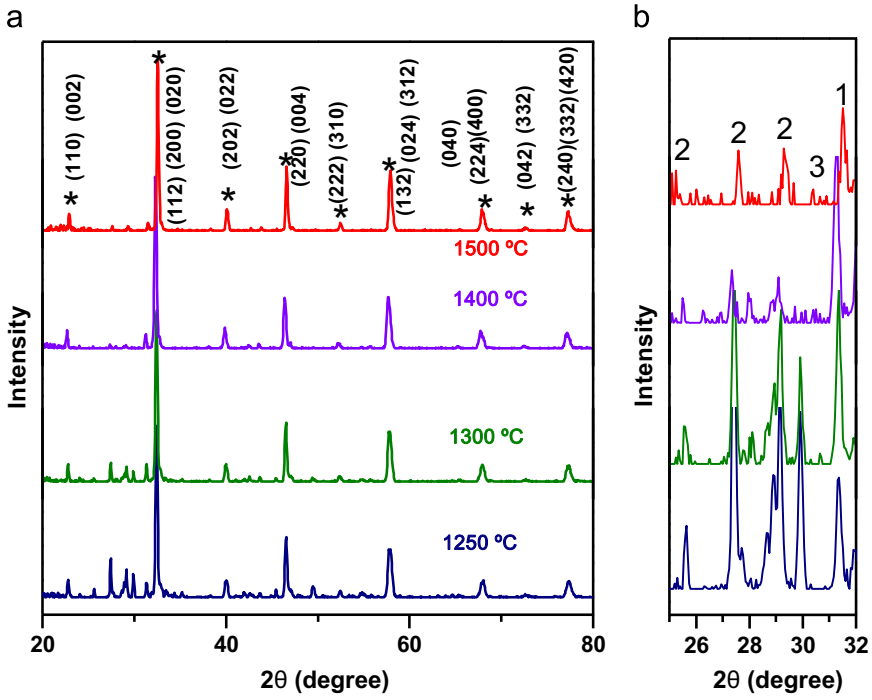

Fig. 1. XRD patterns of LSGM sintered by the TSS method with varying T_1 and null holding time in the (a) 20–80° and (b) 25–32° 2θ ranges. (*) LSGM, (1) $LaSrGaO_4$, (2) $La_4Ga_2O_9$ and (3) $LaSrGa_3O_7$.

Table 1
Values of relative density of LSGM sintered at several T_1 with null holding time and impurity phases: 1-$LaSrGaO_4$, 2-$La_4Ga_2O_9$ and 3-$LaSrGa_3O_7$.

Temperature, T_1 (°C)	Relative density (%)	Impurity phases
1250	59.3	1–2
1300	64.1	1–2
1400	79.0	1–2
1500	98.6	1-2-3

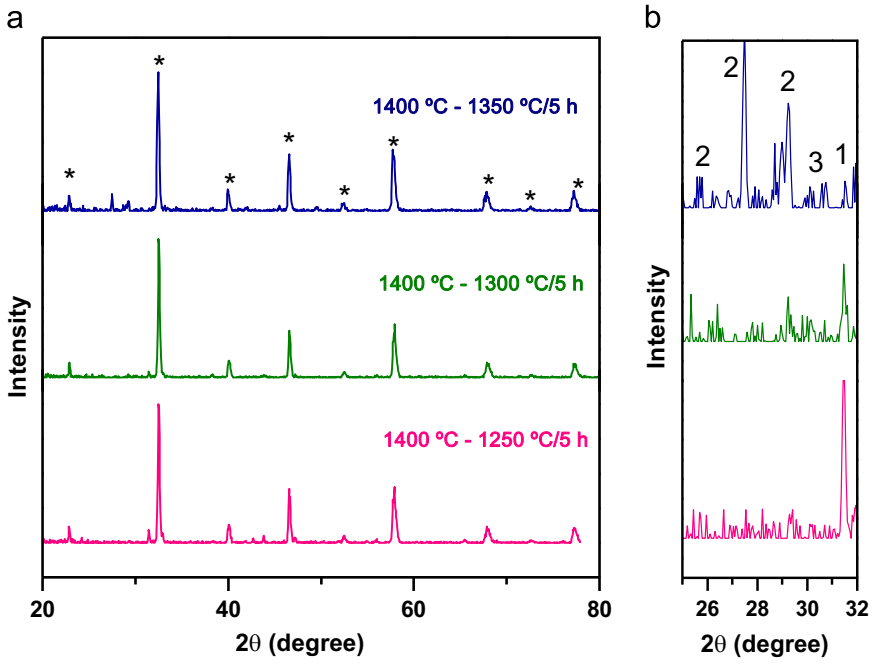

Fig. 2. XRD patterns of LSGM sintered at 1400 °C (T_1) with varying T_2 and t_2 fixed at 5 h in the (a) 20–80° and (b) 25–32° 2θ ranges. (*) LSGM, (1) $LaSrGaO_4$, (2) $La_4Ga_2O_9$ and (3) $LaSrGa_3O_7$.

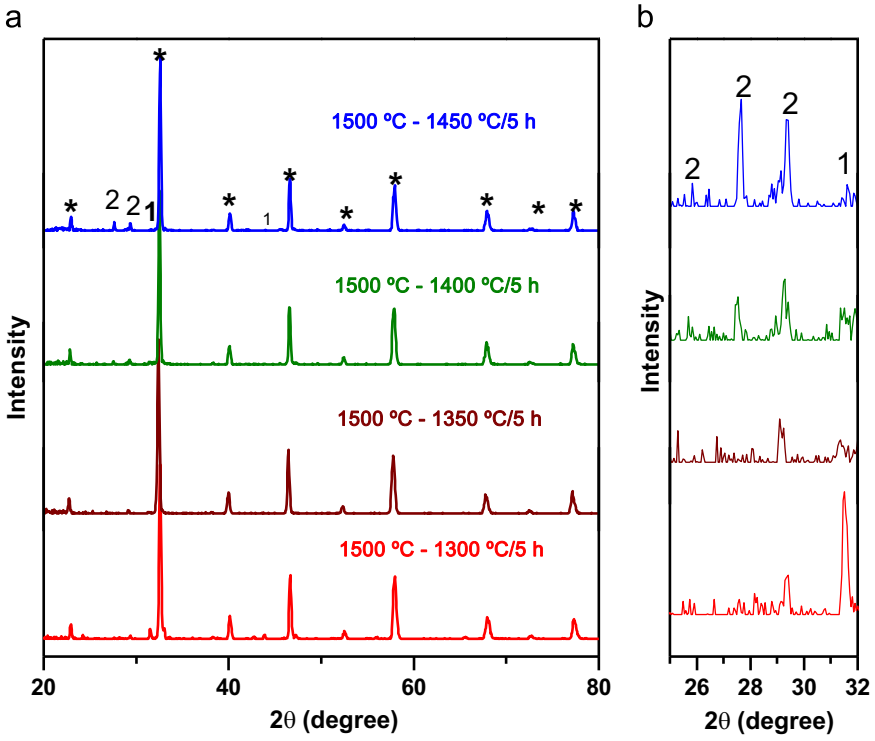

Fig. 3. XRD patterns of LSGM sintered at 1500 °C (T_1) with several T_2 and t_2 fixed at 5 h in the (a) 20–80° and (b) 25–32° 2θ ranges. (*) LSGM, (1) $LaSrGaO_4$, (2) $La_4Ga_2O_9$ and (3) $LaSrGa_3O_7$.

Table 2
Values of relative density and impurity phases of LSGM sintered at several T_2 and t_2 for T_1 of 1400 and 1500 °C. 1-$LaSrGaO_4$, 2-$La_4Ga_2O_9$ and 3-$LaSrGa_3O_7$.

T_1 = 1400 °C			T_1 = 1500 °C		
T_2/t_2 (°C/h)	Relative density (%)	Impurity phases	T_2/t_2 (°C/h)	Relative density (%)	Impurity phases
1250/5	87.8	1–2	1300/5	> 99	1–2
1300/5	94.2	1-2-3	1350/5	> 99	1–2
1350/5	96.9	1-2-3	1400/5	> 99	1–2
			1450/5	> 99	1–2

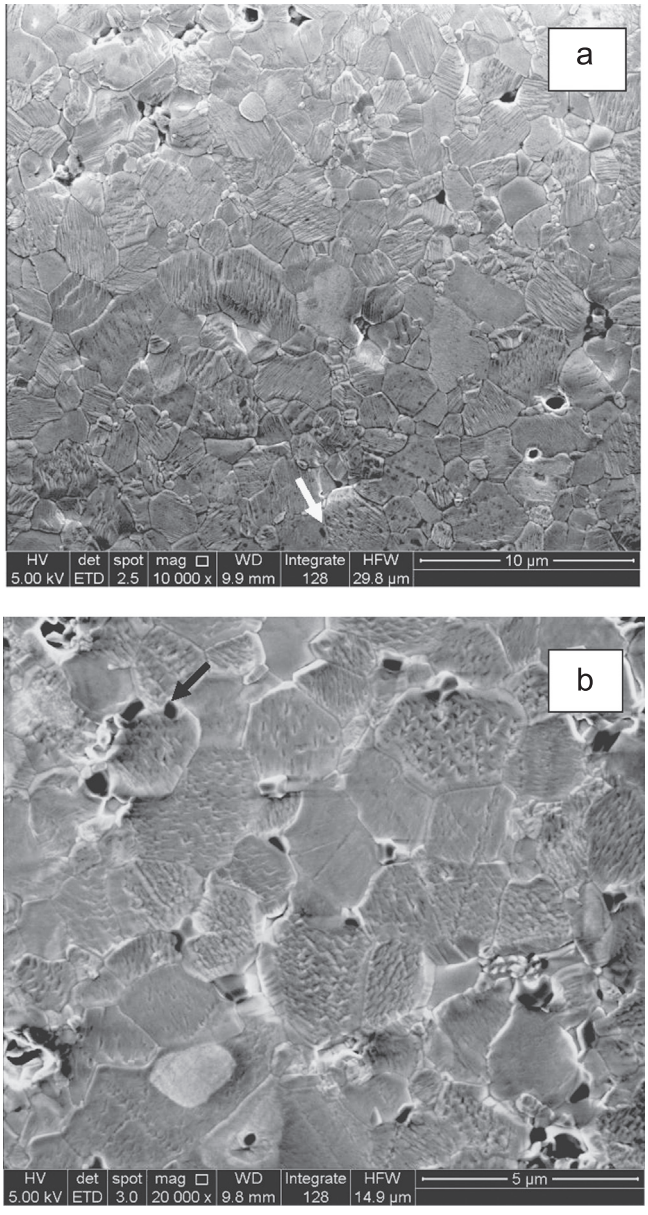

Fig. 4. SEM micrographs of LSGM sintered at (a) 1500 °C with null holding time and (b) 1400 °C followed by 1350 °C for 5 h.

5 Hz-13 MHz and 280–420 °C frequency and temperature ranges, respectively, with 100 mV of applied AC signal. Silver was used as electrode material.

3. Results and discussion

3.1. Density and phase characterization

Green compacts of LSGM were initially sintered at several T_1 to evaluate the effect of this parameter on densification and phase composition. The results are shown in the XRD patterns of Fig. 1a. The orthorhombic structure (space group *Imma*), indexed according to ICSD 51-288, characteristic of this composition, is identified as the predominant phase for all specimens.

The 25–32° angular range of the XRD patterns, where the most intense reflections of impurity phases are detected, is shown in Fig. 1b. The intensities of the main reflections of $LaSrGaO_4$ (1) and $La_4Ga_2O_9$ (2) phases decrease with increasing T_1, indicating that they are formed at low temperatures. This is in general agreement with previous study [24].

In the TSS method, the density attained after T_1 determines the success of the process and the mean grain size [12,13]. Table 1 lists relative density values obtained with several T_1 along with the main impurity phases. It is generally known that in this method of sintering, T_1 is chosen such that a relative density of 75–85% is attained in the first stage. In this case, T_1 should be at least 1400 °C. However, the lower is T_1 the higher is the fraction of impurity phases (Fig. 1). Therefore, we investigated the phase evolution and the electrical conductivity for T_1 of 1400 and 1500 °C.

Fig. 2a shows XRD patterns of LSGM sintered with T_1 of 1400 °C and T_2 between 1250 and 1350 °C (t_2 fixed at 5 h). For these sintering parameters, the fraction of $LaSrGaO_4$ phase decreases with increasing dwell temperature, whereas the $La_4Ga_2O_9$ phase shows the opposite trend. Fig. 2b shows this effect. Relative small fractions of the gallium-rich impurity phase ($LaSrGa_3O_7$, 3) are detected with increasing dwell temperature.

Fig. 3a shows XRD patterns of LSGM sintered with T_1 of 1500 °C, varying T_2 from 1300 to 1450 °C, and t_2 fixed at 5 h. Similar to specimens sintered with T_1 of 1400 °C, in this case also the content of $La_4Ga_2O_9$ increases and that of $LaSrGaO_4$ decreases with increasing T_2. Fig. 3b shows the 25–32° angular range evidencing the minimization of impurity phases for T_2 of 1350 °C. The gallium-rich impurity phase ($LaSrGa_3O_7$) is not identified in these patterns.

These results show that the relative fractions of impurity phases may be controlled by a suitable choice of the sintering profile.

Table 3
Values of mean grain size of LSGM specimens after TSS.

T_1 = 1400 °C		T_1 = 1500 °C	
T_2/t_2 (°C/h)	Mean grain size (μm)	T_2/t_2 (°C/h)	Mean grain size (μm)
1250/5	1.45 ± 0.04	1300/5	3.16 ± 0.07
1300/5	2.11 ± 0.05	1350/5	3.99 ± 0.10
1350/5	2.99 ± 0.06	1400/5	4.21 ± 0.10
		1450/5	4.89 ± 0.12

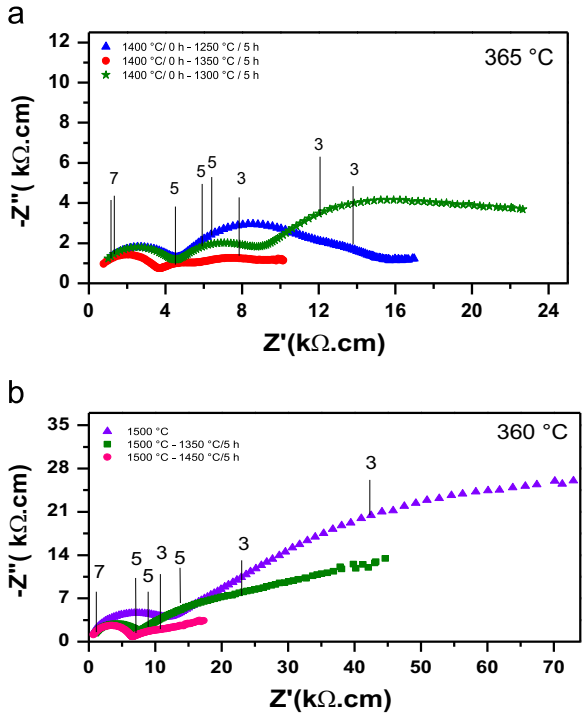

Fig. 5. Impedance spectroscopy diagrams of LSGM sintered at (a) 1400 °C and (b) 1500 °C (T_1) and several T_2 (t_2 = 5 h).

Table 2 shows values of relative density and main impurity phases of the several LSGM specimens. High densification was obtained in all cases, reaching near full density for T_1 of 1500 °C. These values are higher than those reported for the same composition sintered by the conventional method [9,25–27], evidencing the efficiency of the TSS method on densification of LSGM.

3.2. Microstructure and electrical conductivity

The microstructure of LSGM was observed by scanning electron microscopy and few images are shown in Fig. 4 as example. The microstructure of LSGM sintered by this method consists of micrometric grains, with good homogeneity in both shape and size, without abnormal grain growth. Some grains with dark contrast (indicated by arrows) correspond to free MgO, as already reported [28]. This impurity phase is barely detected in conventional XRD measurements due to experimental limitations.

The mean grain size estimated by the intercept method is shown in Table 3. It should be remarked that this microstructure

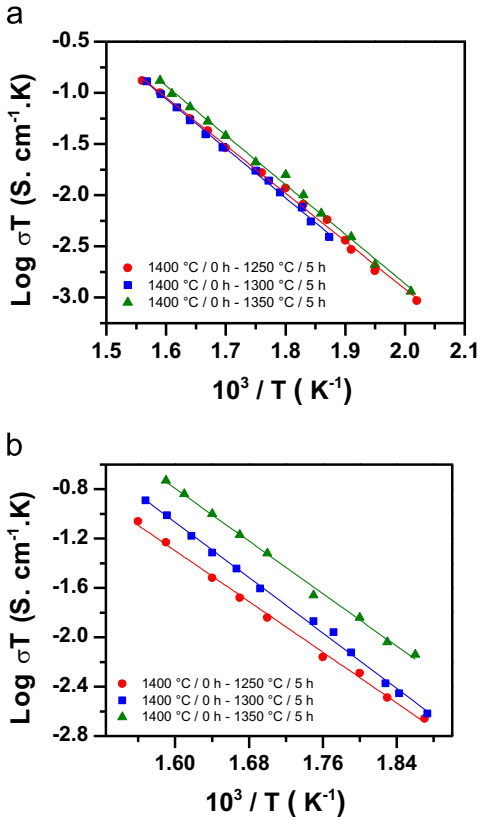

Fig. 6. Arrhenius plots of the (a) grain and (b) grain boundary conductivity of LSGM sintered at 1400 °C (T_1) with several T_2 (t_2 = 5 h).

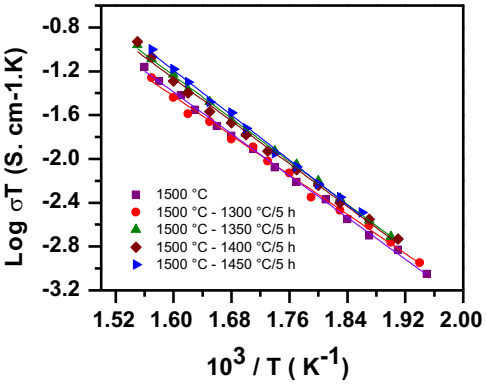

Fig. 7. Arrhenius plots of the grain conductivity of LSGM sintered at 1500 °C (T_1) with several T_2 (t_2 = 5 h).

feature increases with increasing the dwell temperature (T_2) of the isothermal stage. This effect might be related to the relatively high temperature of the first stage. Compared to

previous works, the grain size values determined in this study are larger than those of LSGM sintered by spark plasma [8] and by fast laser solidification [9], smaller than those produced by conventional sintering [27,29,30], and similar to those obtained by fast firing [10].

Impedance spectroscopy measurements were carried out to evaluate the influence of the TSS method on the electrical conductivity of the $La_{0.9}Sr_{0.1}Ga_{0.8}Mg_{0.2}O_{3-\delta}$ solid electrolyte. Fig. 5a shows $-Z''(\omega) \times Z'(\omega)$ plots for specimens sintered with T_1 equal to (a) 1400 and (b) 1500 °C and several T_2. The experimental data was normalized for specimen dimensions for comparison purposes. The impedance diagrams consist of a high frequency arc assigned to the resistive and capacitive effect of the grains, a second arc at intermediate frequencies due to the blocking effect at grain boundaries, which overlaps the low frequency arc due to the electrolyte/electrode interface. The analysis of the impedance diagrams was restricted to the bulk for specimens with T_1 of 1500 °C, because the blocking effect could not be evaluated with accuracy.

Fig. 6 shows Arrhenius plots of LSGM specimens sintered at several dwell temperatures and T_1 of 1400 °C. The grain conductivity (Fig. 6a) is slightly higher for T_2 of 1350 °C, probably because of the expected better homogeneity of the specimen due to the high dwell temperature. The grain boundary conductivity (Fig. 6b) shows the usual trend: the higher is the dwell temperature the higher is the grain boundary conductivity. This effect is attributed to the gradual decrease of the blocking area with increasing the grain size.

Fig. 7 shows Arrhenius plots of LSGM specimens sintered at several (T_2) temperatures and T_1 of 1500 °C. In this case, the evolution of the grain conductivity is shown. It may be seen that specimens sintered only at the first stage (T_1) exhibit slightly lower grain conductivity than those sintered with higher T_2. The same holds for specimens with dwell temperature of 1300 °C (T_2). This result evidences that whenever LSGM is prepared by the solid state reaction method, higher temperatures are required for grain homogeneity and the consequent improvement of the conduction behavior.

The estimated electrical conductivity at 600 °C amounts 12 ($T_1 = 1400$ °C and $T_2 = 1350$ °C) and 8 mS cm^{-1} ($T_1 = 1500$ °C and $T_2 = 1450$ °C), and are higher than those of specimens prepared by spark plasma sintering [8]. Activation energy values for grain and grain boundary conduction are ~1 eV in the temperature range of measurements, and agree with those of previous works [8–10].

The overall results show that a careful choice of sintering parameters of the TSS method allows for controlling and optimizing the microstructure and the electrical conductivity of LSGM.

4. Conclusions

$La_{0.9}Sr_{0.1}Ga_{0.8}Mg_{0.2}O_{3-\delta}$ compounds were successfully consolidated by the two-stage sintering method with high density and good phase purity. Relative density values higher than 99% may be attained by this method of sintering. The overall results show that the two-stage sintering method may be used to minimize the content of impurity phases in LSGM. The mean grain size is lower than those obtained by the conventional method of sintering, ranging from about 1.5–4 μm. The electrical conductivity of specimens sintered with T_1 of 1500 °C shows negligible grain boundary blocking effect. Values of electrical conductivity higher than reported for other methods were obtained.

Acknowledgments

The authors acknowledge FAPESP, Brazil; CNPq, Brazil and CNEN for financial supports. One of the authors (S.L. Reis) acknowledges CNPq (Proc. 505980/2013-4) for the scholarship.

References

[1] K. Huang, R.S. Tichy, J.B. Goodenough, C. Milliken, Superior perovskite oxide-ion conductor; strontium- and magnesium-doped $LaGaO_3$: III, performance tests of single ceramic fuel cells, J. Am. Ceram. Soc. 81 (1998) 2581–2585.

[2] T. Ishihara, M. Honda, Y. Takita, Doped $LaGaO_3$ perovskite type oxide as a new oxide ionic conductor, J. Am. Chem. Soc. 116 (1994) 3801–3803.

[3] M. Feng, J.B. Goodenough, A superior oxide-ion electrolyte, Eur. J. Solid State Inorg. Chem. 31 (1994) 663–672.

[4] E. Djurado, M. Labeu, Second phases in doped lanthanum gallate perovskites, J. Eur. Ceram. Soc. 18 (1998) 1397–1404.

[5] X.C. Lu, J.H. Zhu, Effect of Sr and Mg doping on the property and performance of the $La_{1-x}Sr_xGa_{1-y}Mg_yO_{3-\delta}$, J. Electrochem. Soc. 155 (2008) B494–B503.

[6] K. Huang, M. Feng, J.B. Goodenough, Wet chemical synthesis of Sr- and Mg-doped $LaGaO_3$, a perovskite-type oxide-ion conductor, J. Am. Chem. Soc. 79 (1996) 1100–1104.

[7] S. Li, B. Bergman, Doping effect on secondary phases, microstructure and electrical conductivities of $LaGaO_3$ based perovskites, J. Eur. Ceram. Soc. 29 (2009) 1139–1146.

[8] B. Liu, Y. Zhang, $La_{0.9}Sr_{0.1}Ga_{0.8}Mg_{0.2}O_{3-\delta}$ sintered by spark plasma sintering (SPS) for intermediate temperature SOFC electrolyte, J. Alloy. Compd. 458 (2008) 383–389.

[9] J. Zhang, E.J. Liang, X.H. Zhang, Rapid synthesis of $La_{0.9}Sr_{0.1}Ga_{0.8}Mg_{0.2}O_{3-\delta}$ electrolyte by a CO_2 laser and its electric properties for intermediate temperature solid state oxide full cells, J. Power Sources 195 (2010) 6758–6763.

[10] S.L. Reis, E.N.S. Muccillo, Ionic conductivity of chemically synthesized $La_{0.9}Sr_{0.1}Ga_{0.8}Mg_{0.2}O_{3-\delta}$ solid electrolyte, Adv. Mater. Res. 965 (2014) 81–85.

[11] I.-W. Chen, X.-W. Wang, Sintering dense nanocrystalline ceramics without final-stage grain growth, Nature 404 (2000) 168–171.

[12] Y.-I. Lee, Y.-W. Kim, M. Mitomo, D.-Y. Kim, Fabrication of dense nanostructured silicon carbide ceramics through two-step sintering, J. Am. Ceram. Soc. 86 (2003) 1803–1805.

[13] Y.-I. Lee, Y.-W. Kim, M. Mitomo, D.-Y. Kim, Effect of processing on densification of nanostructured SiC ceramics fabricated by two-step sintering, J. Mater. Sci. 39 (2004) 3801–3803.

[14] H.T. Kim, Y.H. Han, Sintering of nanocrystalline $BaTiO_3$, Ceram. Int. 30 (2004) 1719–1723.

[15] H.D. Kim, Y.-J. Park, B.-D. Han, M.-Q. Park, W.-T. Bae, Y.-W. Kim, H.-T. Lin, P.F. Becher, Fabrication of dense bulk nano-Si_3N_4 ceramics without secondary crystalline phase, Scr. Mater. 54 (2006) 615–619.

[16] K. Bodisová, P. Sajgalik, G. Galusek, P. Svancarek, Two-stage sintering of alumina with submicrometer grain size, J. Am. Ceram. Soc. 90 (2007) 330–332.

[17] M. Mazaheri, A.M. Zahedi, S.K. Sadrnezhaadt, Two-step sintering of nanocrystalline ZnO compacts: effect of temperature on densification and grain growth, J. Am. Ceram. Soc. 91 (2008) 56–63.
[18] J. Binner, K. Annapoorani, A. Paul, I. Santacruz, B. Vaidhyanathan, Dense nanostructured zirconia by two stage conventional/hybrid microwave sintering, J. Eur. Ceram. Soc. 28 (2008) 973–977.
[19] D.-S. Kim, J.-H. Lee, R.J. Sung, W.W. Kim, H.S. Kim, J.S. Park, Improvement of translucency in Al_2O_3 ceramics by two-step sintering, J. Eur. Ceram. Soc. 27 (2007) 3629–3632.
[20] G. Magnani, A. Brentari, E. Burresi, G. Raiteri, Pressureless sintered silicon carbide with enhanced mechanical properties obtained by the two-step sintering method, Ceram. Int. 40 (2014) 1759–1763.
[21] K. Maca, V. Pouchly, P. Zalud, Two-step sintering of oxide ceramics with various crystal structures, J. Eur. Ceram. Soc. 30 (2010) 583–589.
[22] A. Nadernezhad, F. Moztarzadeh, M. Hafezi, H.B. Bafrooei, Two step sintering of a novel calcium magnesium silicate bioceramic: sintering parameters and mechanical characterization, J. Eur. Ceram. Soc. 34 (2014) 4001–4009.
[23] M.J. Mendelson, Average grain size in polycrystalline ceramics, J. Am. Ceram. Soc. 52 (1969) 443–446.
[24] M. Rozumek, P. Majewski, L. Sauter, F. Aldinger, Homogeneity region of strontium- and magnesium-containing $LaGaO_3$ at temperatures between 1100° and 1500 °C in air, J. Am. Ceram. Soc. 86 (2003) 1940–1946.
[25] Raghvendra, R.K., Singh, P. Singh, Influence of small DC bias field on the electrical behaviour of Sr- and Mg-doped lanthanum gallate, Appl. Phys. A 116 (2014) 1793–1800.
[26] A.-M. Azad, L.F. Er, Microstructural evolution in B-site Mg-substituted $La_{0.9}Sr_{0.1}GaO_{3-\delta}$ oxide solid solutions, J. Alloy. Compd. 306 (2000) 103–112.
[27] Y.-C. Wu, M.-Ze Lee, Properties and microstructural analysis of $La_{1-x}Sr_xGa_{1-y}Mg_yO_{3-\delta}$ solid electrolyte ceramic, Ceram. Int. 39 (2013) 9331–9341.
[28] R. Polini, A. Pamio, E. Traversa, Effect of synthetic route on sintering behaviour, phase purity and conductivity of Sr- and Mg-doped $LaGaO_3$ perovskites, J. Eur. Ceram. Soc. 24 (2004) 1365–1370.
[29] J. Drennan, V. Zelizko, D. Hay, F.T. Ciacchi, S. Rajendran, S.P. S. Badwal, Characterisation, conductivity and mechanical properties of the oxygen-ion conductor $La_{0.9}Sr_{0.1}Ga_{0.8}Mg_{0.2}O_{3-x}$, J. Mater. Chem. 7 (1997) 79–83.
[30] K. Huang, R.S. Tichy, J.B. Goodenough, Superior perovskite oxide-ion conductor; strontium- and magnesium-doped $LaGaO_3$: II, ac impedance spectroscopy, J. Am. Ceram. Soc. 81 (1998) 2576–2580.